Universal Journal of Lasers, Optics, Photonics & Sensors (UJLOPS)
UINUJLOPS003/ William (Doc A) Arrasmith

ETEXT

# Diversity-based Atmospheric Turbulence Compensation for Incoherent Imaging Systems using a New Well Optimized Linear Finder Methodology

William (Doc A) Arrasmith, PhD
Florida Institute of Technology, Melbourne, FL, USA

**Received:** 4 June 2021; **Accepted:** 18 June 2021; **Published:** 21 June 2021

**Citation:** William (Doc A) Arrasmith. Diversity-based Atmospheric Turbulence Compensation for Incoherent Imaging Systems using a New Well Optimized Linear Finder Methodology (2021): 12-20.

**ABSTRACT**

A new high-speed, high-accuracy general transfer function estimation method for diversity-based blind deconvolution problems is presented that has been found to be faster and more accurate than traditional methods used in transfer function estimation/blind-deconvolution problems such as removing atmospheric turbulence from coherent and incoherent optical imagery. Our new Well Optimized Linear Finder (WOLF)method applies across the electromagnetic and acoustic spectrum and benefits any linear/linear shift-invariant (or linearizable) system where channel aberrations can be well-modeled as phase aberrations, and diversity-based methods can be used to converge a suitable error-metric. We present an overview of the WOLF paradigm and demonstrate its performance on a 256 x 256 aberration-simulated image with additive Gaussian noise. We show that atmospheric aberrations and Gaussian noise can be removed from the image in about 8 seconds using an un-optimized and non-parallel version of the WOLF methodology.

## INTRODUCTION

In the field of optical imaging, if a well-designed (low noise) imaging system has an aperture that is larger than the atmospheric coherence length, $r_0$, the greatest source of aberrations and degradation of spatial resolution performance stems from the turbulence in the atmosphere [1-3]. Other causes of loss in spatial resolution include the choice of operating wavelength (the larger the wavelength(s) the lower the attainable spatial resolution), the relative size of the imaging system's entrance pupil diameter, the atmospheric coherence length, $r_0$ (Fried parameter), the angular instantaneous field of view (IFOV), the isoplanatic angle, $\theta_i$, spatial sampling effects, signal-to-noise issues, and system effects such as imperfect optics, imaging system noise and platform jitter [4-6]. To minimize the impact of atmospheric turbulence on incoherent (passive) imaging systems, three approaches have in general been developed: 1) Adaptive Optics (AO)

systems, 2) Atmospheric Turbulence Compensation (ATC) systems, and 3) Hybrid systems [7-13]. The AO systems tend to be complex, fragile, and expensive but can often be run in real-time (corrections faster than 60 Hz). Traditional ATC methods are post-processing approaches that are mostly implemented in software but tend to take a long time to remove the atmospheric turbulence (hours to days for some relatively small image segments/images, say 64x64 pixels). The Hybrid systems are a mix of the AO and ATC methods. What is common to all these methods is that they attempt to remove the effects of atmospheric aberrations from optical imagery. In the next section, we provide an overview of the WOLF methodology. In the following section we provide a computational example. In the last section we provide our conclusions.

## ANALYSIS

A linear, shift invariant imaging model can be applied to a wide variety of incoherent imaging problems[1, 14]. The theoretical and mathematical model for an incoherent imaging system is given by,

$$(\vec{x}) = (\vec{x}) * |h\,(\vec{x})\,|^2, \tag{1}$$

where $o(\vec{x})$ is the un-aberrated radiant emittance (object brightness function), $h_i(\vec{x})$ is the impulse response, $|h_i(\vec{x})|^2$ is the imaging system's point spread function (PSF) and $i(\vec{x})$ is the aberrated image due to atmospheric and optical imaging system effect, $(\vec{x})$ is a 2D position vector and the asterisk represents 2D spatial convolution. Because of the Taylor's frozen flow assumption leading to a very short camera integration time, and since for single aperture systems we are interested in only relative phase and not absolute phase, we can drop the time dependence from our analysis and only consider spatial (or equivalently spatial frequency) effects. Taking the 2D Fourier transform of Equation (1) and normalizing the result by dividing by the maximum value of the unnormalized OTF leads to Equation (2), which is the well-known frequency space equivalent of Equation (1),

$$I(\vec{f}) = O(\vec{f})\mathcal{H}(\vec{f}). \tag{2}$$

Here $(\vec{f})$ is the image spectrum, $(\vec{f})$ is the object spectrum and $\mathcal{H}$ $(\vec{f})$ represents the optical transfer function (OTF). In Equation (2), $(\vec{f})$ is a 2D spatial frequency variable. Equations (1) and (2) apply at each spatial coordinate $\vec{x}$ and spatial frequency $\vec{f}$. The Generalized Pupil Function (GPF) is given by,

$$W(\vec{x}) = A(\vec{x})e^{j\theta(\vec{x})}. \tag{3}$$

In Equation (3), $(\vec{x})$ is an amplitude function. However, for the case of near-field atmospheric turbulence such as in a ground-to-air/space optical imaging system, the amplitude becomes one inside of the clear aperture of the imaging system and zero everywhere else. In equation (3), $(\vec{x})$ is the atmospherically induced phase aberration realized at spatial coordinate $(\vec{x})$ in the entrance pupil of the imaging system.

In diversity-based traditional ATC methods, a common method is to insert some sort of known diversity into the system and simultaneously capture the original image and the diversity image [15-17]. The OTFs of the aberrated and diversity images are then mathematically related to each other based on known physical relationships, and then an error metric is used to select the OTF that produces the lowest local and global error. As an example of a known physical relationship, the well-understood phase-diversity method uses an additive phase term that can be obtained ahead of time in the expression of the phase diversity generalized pupil function,

$$W_{pd}(\vec{x}) = A(\vec{x})e^{j(\theta(\vec{x})+\theta_{pd}(\vec{x}))}. \tag{4}$$

Here $(\vec{x})$ represents the a priori known and introduced phase diversity term at entrance pupil plane spatial position $(\vec{x})$. The OTF can be calculated directly from the GPF from the following equation,

$$\mathcal{H}(\vec{f}) = \frac{(\vec{x}) \otimes W(\vec{x})}{(0) \quad (\vec{0})}, \tag{5}$$

where, $\otimes$, represents the autocorrelation process. The entrance pupil plane spatial position variable isrelated to the spatial frequency by,

$$\vec{x} = \lambda d_i \vec{f}. \tag{6}$$

A similar expression to Equation (5) is generated for the diversity OTF by replacing the GPF shown in Equation (3) with the diversity GPF shown in Equation (4). In many ATC methods, the task is to use the OTF and the diversity OTF with a suitable error metric to first estimate the entrance pupil plane phases due to the atmospheric aberrations, use the phases to determine the OTF, determine the OTF inverse, and recover the object brightness estimate by multiplying Equation (2) by the inverse OTF at every point to determine the object spectrum. Finally, the estimate of the object radiant emittance is obtained by inverse 2D Fourier transforming the estimated object spectrum. We now present a brief overview of the WOLF methodology.

We generally use a square entrance pupil in our development instead of the more typical

circular entrance pupil because the square entrance pupil can contain other types of apertures within its boundaries (e.g., circular, hexagonal, octagonal shaped apertures). For camera systems with many samples across the entrance pupil horizontally, $N_p$, and vertically, $M_p$, a third dimension exists that can have up to millions of elements making the autocorrelation of the GPF scale as $(2N_p - 1)$ $(2M_p - 1)$ for a rudimentary square sampled entrance pupil. As an example, for a 16-million-pixel square aperture camera, the image produced would be 4000x4000 pixels. The corresponding maximum entrance pupil would be found by relating the value of $(2N_p - 1) = 4000$ and $(2M_p - 1) = 4000$, each coming to roughly 2000 samples. The third dimension, L, is associated with up to a maximum number of complex exponential phase difference sums of order $(N_p)(M_p)$. In other words, practically every pixel has associated with it a vector of variable length (from 1 to $(N_p * M_p)$ elements long) that consists of sums of normalized complex exponential phase differences related to the OTF. This makes the computation of the autocorrelation of the GPF a $(2N_p - 1)(2M_p - 1)L$ problem where $L$ can range from 1, up to 4 million in the given example. For a visual representation, and to understand the concepts behind the WOLF paradigm, we use Figure 1 to provide a useful illustration. In implementing Equation (5), we see that the numerator is basically a 2D autocorrelation of the GPF. For a square entrance pupil aperture this can be shown by the fixed array shown in blue, and a moving array shownin green.

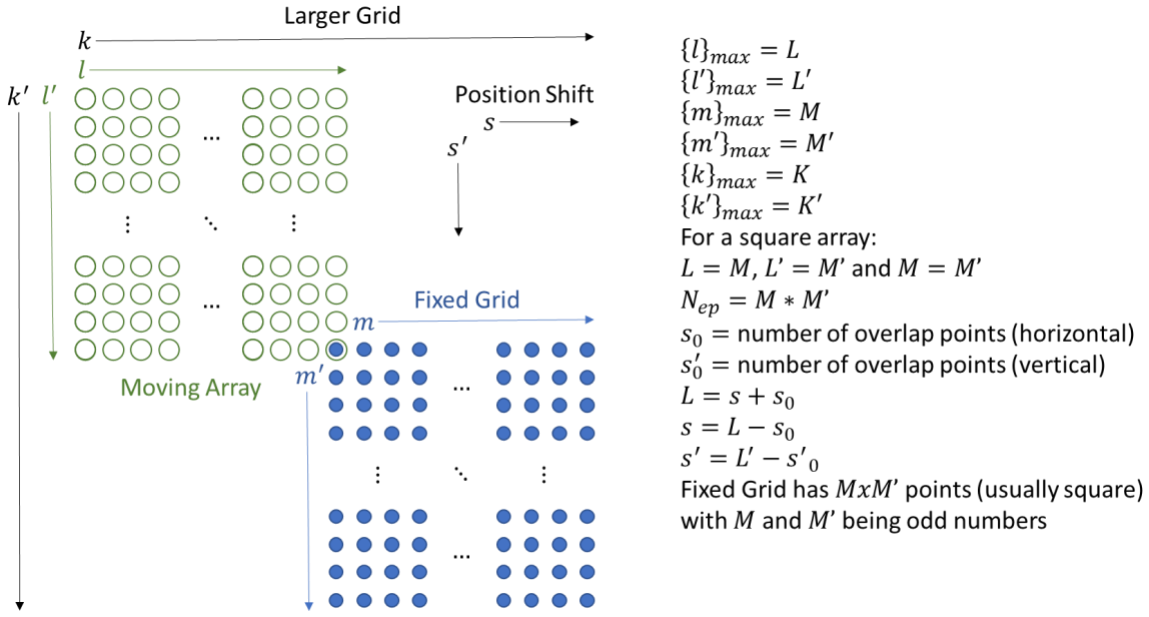


*Figure 1: 2D Spatial Autocorrelation of the Generalized Pupil Function (one-point overlap)*

In this illustration the first non-zero element of the spatial autocorrelation carried out in Equation (5) involves the top-left point of the blue fixed array, and the bottom-right point of the moving green array. The coordinates show the non-primed values for horizontal elements of the array, and primed values for the vertical elements. Capital letters represent maximum values. The entrance pupil plane vertical and horizontal indices for the green

moving array are *(l', l)* respectively. For the fixed blue array the coordinates are (m', m), and the large array representing the OTF is given by *(k', k)*. For the one-point overlap shown in Figure 1, the OTF point that is being solved is at the center of the green grid. Typically, an odd number of samples are chosen for the entrance pupil plane grid in each spatial direction so that the center point falls in the middle of the grid. The algorithm WOLF_Tau is used to solve the one-point overlap case for any unknown entrance pupil plane phase, the complex value of the OTF at the center of the green moving grid, and the corresponding object radiant emittance magnitude and phase. The WOLF paradigm then proceeds to solve the next point in the OTF by moving the green array one point to the right. As seen in Figure 1, this produces a two-point overlap between the moving green array and the fixed blue array. The algorithm WOLF_Iota is used to solve the two-point overlap problem for either horizontal or vertical overlapping of two points. WOLF_Iota produces the unknown entrance pupil plane phases, the value of the OTF itself at the distinct two-point overlap OTF coordinate, and simultaneously the corresponding object spectrum magnitude and phase. Proceeding on to three or more points, WOLF_Alpha is the primary algorithm used to calculate the needed entrance pupil, OTF, and object parameters. It is interesting to note that the same WOLF_Alpha algorithm can be used to solve for any three "or more" overlapping points in the autocorrelation expression shown in Equation (5). Said in another way, regardless of how many points overlap in the autocorrelation carried out in the numerator of Equation (5), the terms can be arranged so that there are no more than two unknown phase terms with a single knowable complex constant that reduces to an equivalent 3-point overlap problem which is solvable by the application of WOLF_Alpha. This is because Arrasmith found that each OTF point can be independently solved from each other and that the solutions to preceding points (e.g., the solutions of the 1-point and 2-point problems when considering a 3-point overlap problem) ensured that there were no more than two unknown entrance pupil plane phases and a reduced single, complex, known, constant for the next OTF point that is evaluated. Additionally, Arrasmith also noted that for single processor computing systems, because of symmetry conditions in the OTF, only up to half of the entrance pupil plane points need to be incrementally overlapped to fully determine all the entrance pupil plane phases, and consequently the full OTF. For a dual-processor computing system, only up to a quarter of the entrance pupil plane points need to be evaluated by any single processor. This means that the OTF can be directly determined according to Equation (5) by a single pass for each processor of no more than a quarter of the size of the entrance pupil, and that at each point, the computation complexity can be reduced to no more than the sum of 2 complex exponential phase differences with a known complex constant (versus the sum of millions of complex exponential phase differences in previous methods). To gain this computational advantage, the OTF points need to be solved in a sequential order (1-point overlap leading to 2-point overlap, 2-point overlap leading to 3-point overlap and so forth) and then "stitched" together. The details can be found in [18].

For the 16-million-pixel example above with a square entrance pupil of odd dimensions, the computational problem using the WOLF paradigm would scale as no more than $(\frac{(Np+1)}{2})(\frac{(Mp+1)}{2}) * 3$ or roughly 3 million 2 2 complex exponential phase difference sums using 2 General Purpose Parallel Processors (GPPPs). When combined with additional parallel processing elements such as a Graphics Processor Unit (GPU) or

Field Programmable Gate Array (FPGA) and the employment of pre-determined lookup tables (LUT) the computational complexity of this method will be further substantially reduced.

## RESULTS

In this section, we provide some results of our WOLF algorithm on simulated atmospheric turbulence degraded imagery that uses a realistic atmospheric realization based on the Kolmogorov power spectrum. We used Figure 2 below as our reference (Truth) object radiant emittance. Consistent with our development above, we use a square entrance pupil plane with 127 by 127 samples. This size aperture leads to a 256 x 256 OTF and image. The Truth Radiant Emittance has units of Watts/meter-squared and represents our un-aberrated object.


*Figure 2: Representative Truth Radiant Emittance*

Looking closely at the Truth Object, a lot of spatial detail can be observed. This is particularly noticeable in the edge of the hat, the plume, hair, and eyes of our representative object. Our Truth Object ($\vec{x}$) is Fourier transformed to produce the object spectrum ($\vec{f}$). The object spectrum will eventually be point-wise multiplied with the Optical Transfer Function $\mathcal{H}(\vec{f})$ and Diversity Optical Transfer Function $\mathcal{H}_d(\vec{f})$ to produce the image spectrum and diversity image spectrum. The image spectrum and diversity image spectrum are respectively inverse Fourier transformed to get the simulated aberrated image and aberrated diversity image. These pair of images, along with some a priori imaging parameters such as the aperture diameter size, number of entrance pupil samples, effective focal length of the imaging system, are the inputs to the WOLF algorithm. Note that in real-world applications, the image and diversity image are

obtained from field measurements and the WOLF algorithm is used to estimate and remove the aberrations generated by the atmosphere without any additional information besides the image system parameters known ahead of time.

To generate a realization of entrance pupil plane phases that accurately reflects the Earth's atmosphere, we use the methods described by Roggemann and Welsh, in their seminal work, Imaging Through Turbulence, by CRC press [1]. We use the Kolmogorov representation of the power spectral density (PSD) in this example since we are assuming a single aperture imaging system with one image pair (image and diversity image). We assume Taylor's frozen flow approximation to essentially "freeze" the atmospheric realization so that we can subsequently undo the atmospheric effects represented by the entrance pupil plane phases. The practical implication is that the imaging system's integration time needs to be on the order of 2 milliseconds or less. If video is being corrected for atmospheric effects, then each image frame must have an integration time of no more than a few milliseconds. In generating the model for the entrance pupil plane phases, the Kolmogorov PSD is used to generate the covariance matrix of Zernike basis function "weights." A zero-mean, unit variance Gaussian random vector is generated and used with the amplitude covariance matrix to generate a realization of the Zernike basis function amplitudes that has the correct atmospheric statistics (inherent in the covariance matrix of the weights). The appropriate amplitude realizations are combined with the corresponding Zernike basis functions and the results are summed together to produce the entrance pupil plane phase realization with correct atmospheric statistics. Figure 3 below shows the result of this process.

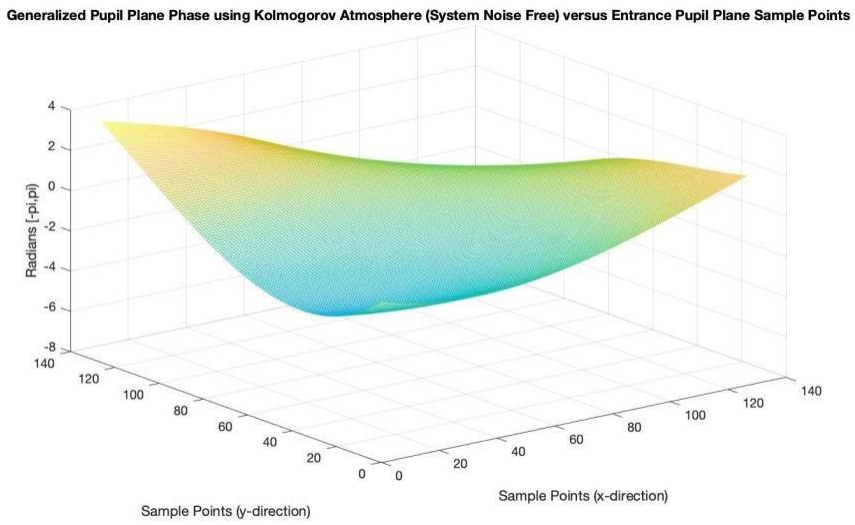


*Figure 3: Entrance Pupil Plane Generated Phase Realization*

We next added zero-mean Gaussian white noise to the phase with a magnitude of a tenth of a radian to represent channel noise. Figure 4 shows our result. As can be seen, this is a significant amount of noise added to our phase estimates and the resulting entrance pupil plane phase map embodies both atmospheric and additive channel effects.

ETEXT

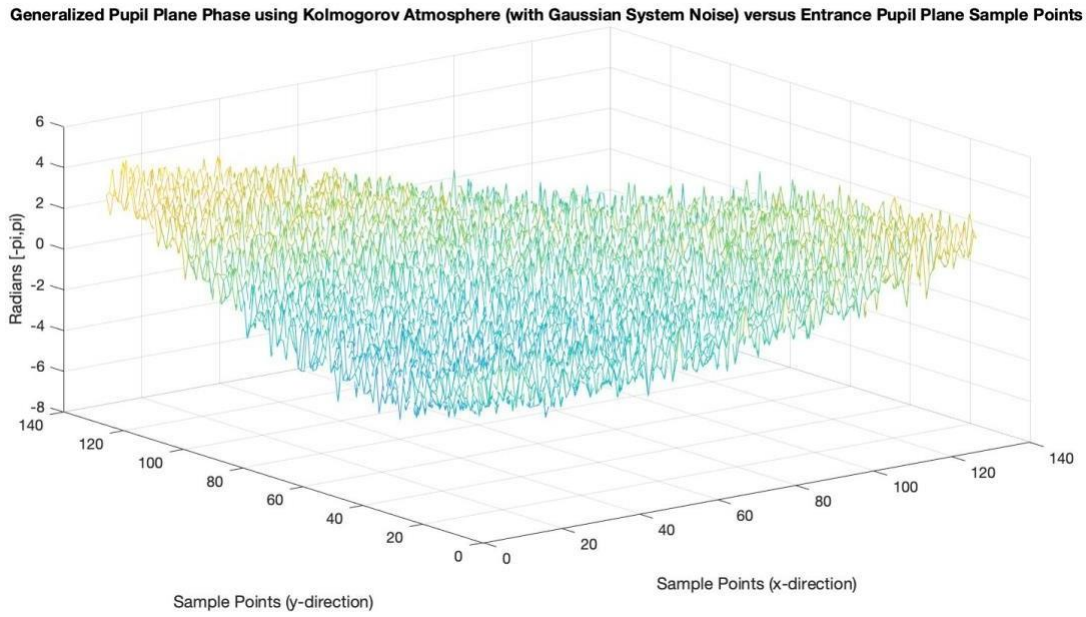


*Figure 4: Entrance pupil plane phase realization with additive Gaussian white noise*

Figure 5 shows the modulation transfer function (MTF) which is obtained by taking the magnitude of the OTF generated using Kolmogorov-based entrance pupil plane phases on our square aperture. This shows the effects of the atmosphere on the magnitude of the OTF. Note the channels carved into the MTF by the phase aberrations.

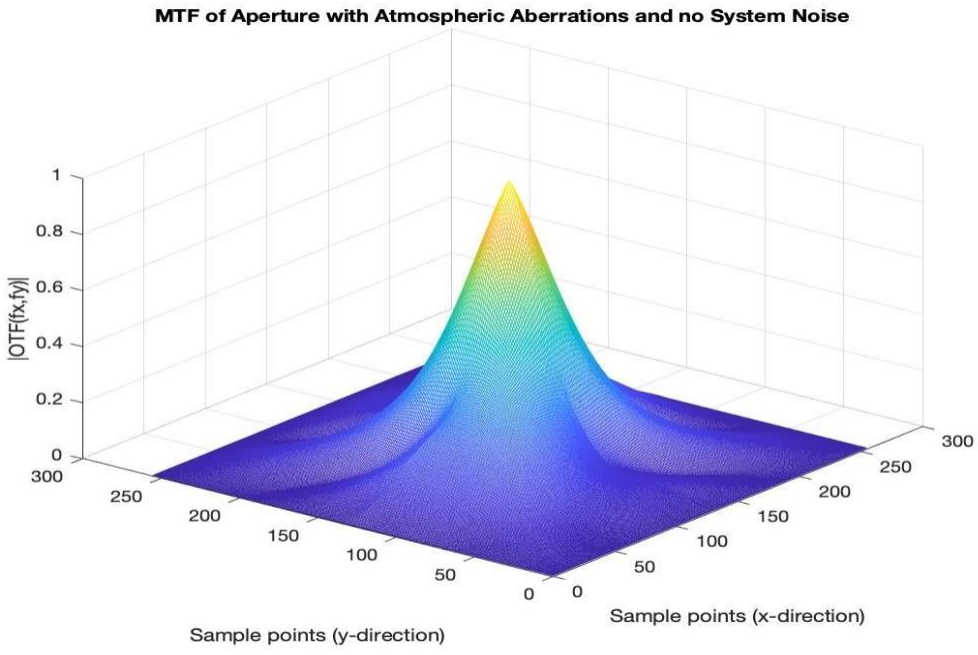


*Figure 5: MTF associated with the image*

Figure 6 shows the MTF associated with the image in the presence of one tenth of a wave of Gaussian white noise. Notice the rapid drop off of the MTF around the central peak of the MTF.

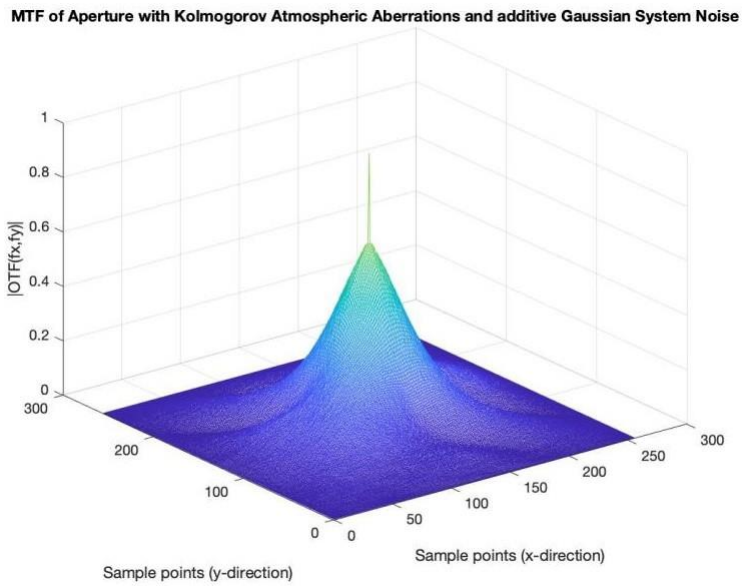


*Figure 6: MTF associated with the image with additive Gaussian white noise*

Figure 7 shows our simulated aberrated image that we obtain by applying the OTF generated with our Kolmogorov-based atmospheric phase realization and includes the channel noise effects (one tenth wave of additive white Gaussian noise). This image represents what would be received at the detector and displays atmospheric aberrations, aperture, and channel noise effects.


*Figure 7: Aberrated image with additive Gaussian white noise*

Figure 8 shows the reconstructed object radiant emittance after applying our WOLF methodology. Our method requires only the detected image, diversity image, and imaging

system parameter information that is known in advance to estimate the OTF, diversity OTF, entrance pupil plane phases and entrance pupil plane diversity phases, and in turn recovers the un-aberrated object radiant emittance by inverse 2D Fourier transforming the recovered object spectrum.


*Figure 8: Reconstructed object radiant emittance using the WOLF method*

Notice that even for a relatively strong amount of additive Gaussian noise, the WOLF method is capable of completely removing the atmospheric aberrations and the Gaussian noise effects. After consideration, this is expected given a sufficiently accurate sampling strategy since the WOLF method is in essence a "point estimator" and corrects for the total combined phase aberrations at every distinct point of the OTF and consequently at every distinct point of the imaging systems entrance pupil. This image took approximately 8 seconds to render on a 2014 MacBook Pro computer with a 2.8 GHz Quad-Core Intel Core i7 processor with 16 GB of 1600 MHz DDR3 memory and running Matlab 2020b with an un-optimized, non-parallel version of the WOLF methodology. The only inputs where the aberrated image and the aberrated diversity image.

## CONCLUSION

We applied simulated atmospheric turbulence to a pair of 256 by 256 images (image and diversity image) and showed that on a somewhat dated (2014) ordinary MacBook Pro computer, the non-optimized, non- parallel implementation of the WOLF paradigm can reconstruct the turbulence free, and channel noise-free, diffraction-limited image in approximately 8 seconds. Our WOLF method is implementable using parallel processing technologies such as the Graphical Processing Unit (GPU) on a conventional laptop computer and/or Field Programmable Gated Array technologies with expected real-time (faster than 30 Hz) performance for software-dominant transfer function estimation/blind deconvolution/atmospheric turbulencecompensation problems.

## REFERENCES

ETEXT

1. M. C. Roggemann, B. Welsh: *Imaging through Turbulence*, CRC Press, New York, 1996.
2. F. Roddier, "The effects of atmospheric turbulence in optical astronomy," *Progress in Optics* (E. Wolf,ed.), North-Holland, Amsterdam, Vol. 19, p283-369, 1981.
3. R. K. Tyson, *Principles of Adaptive Optics*, Academic Press, Boston, 1991.
4. D. L. Fried, "Optical Resolution Through a Randomly Inhomogeneous Medium for Very Long and VeryShort Exposures," *J. Opt. Soc. Am.*, Vol 56, p1372-1379.
5. J. W. Goodman, *Statistical Optics*, J. Wiley, New York, 1985.
6. J. W. hardy, "Active Optics: A new technology for the control of light," *Proc. IEEE*. Vol. 66, p651-697,1978.
7. D. Korff, "Analysis of a method for obtaining near-diffraction-limited information in the presence ofatmospheric turbulence," *J. Opt. Soc. Am.*, Vol. 63, p971-980, 1973.
8. R. A. Gonsalves and R. Chidlaw, "Wavefront Sensing by Phase Retrieval," *Proc. On Applications ofDigital Image Processing III*, SPIE, Vol. 207, 1979.
9. S. W. Paine and J. R. Fienup, "Machine learning for improved image-based wavefront sensing," *Opt.Lett.*, Vol. 43, p1235–1238, 2018.
10. H. R. Ingleby and D. R. McGaughey, "Parallel multiframe blind deconvolution using wavelengthdiversity," *Proc. of Image Reconstruction from Incomplete Data III*, SPIE, Vol. 5562, p58-64, 2002.
11. M. C. Roggemann and C. L. Matson, "Partially compensated speckle imaging: Fourier phase spectrumestimation," Proc. SPIE, Vol. 2542, 1991.
12. T. Schultz, "Multiframe blind deconvolution of astronomical images," *J. Opt. Soc. Am.*, Vol. 10, Issue5, p1064-1073, 1993.
13. R. G. Paxman and J. R. Fienup, "Optical misalignment sensing and image reconstruction using phasediversity," *J. Opt. Soc. Am.*, Vol. 5, No. 6, p914-923, 1988.
14. J. W. Goodman, *Introduction to Fourier Optics*, McGraw-Hill, New York, 1968.
15. R. A. Gonsalvez, "Phase Retrieval and Diversity in Adaptive Optics," J. of Optical Engineering, Vol.21, Num. 5, 1982.
16. R. G. Paxman, T. J. Schulz, and J. R. Fienup, "Joint estimation of object and aberrations by usingphase diversity," *JOSA A 9*, p1072–1085, 1992.
17. M. K. Sharma, C. Gaur, P. Senthilkumaran, and K. Khare, "Phase imaging using spiral-phasediversity," *Appl. Opt.*, Vol. 54, p3979–3985, 2015.
18. W. W. Arrasmith, "High-speed Diversity-based Imaging Method for Parallel Atmospheric TurbulenceCompensation," U.S. patent number: US 8,447,129 B2, May 21, 2013.